Two-beam pumped cascaded four-wave-mixing process for producing multiple-beam quantum correlation

Shengshuai Liu,[1] Hailong Wang,[1] and Jietai Jing[1,2,3,*]

[1]*State Key Laboratory of Precision Spectroscopy, School of Physics and Materials Science, East China Normal University, Shanghai 200062, China*

[2]*Department of Physics, Zhejiang University, Hangzhou 310027, China*

[3]*Collaborative Innovation Center of Extreme Optics, Shanxi University, Taiyuan, Shanxi 030006, People's Republic of China*

(Received 25 November 2017; published 19 April 2018)

We propose a two-beam pumped cascaded four-wave-mixing (CFWM) scheme with a double-Λ energy-level configuration in ^{85}Rb vapor cell and experimentally observe the emission of up to 10 quantum correlated beams from such CFWM scheme. During this process, the seed beam is amplified; four new signal beams and five idler beams are generated. The 10 beams show strong quantum correlation which is characterized by the intensity-difference squeezing of about -6.7 ± 0.3 dB. Then, by altering the angle between the two pump beams, we observe the notable transition of the number of the output beams from 10 to eight, and even to six. We find that both the number of the output quantum correlated beams and their degree of quantum correlation from such two-beam pumped CFWM scheme increase with the decrease of the angle between the two pump beams. Such system may find potential applications in quantum information and quantum metrology.

DOI: 10.1103/PhysRevA.97.043846

I. INTRODUCTION

Four-wave mixing (FWM) is a nonlinear effect arising from a third-order optical nonlinearity, in which the photons in pump beams can be converted into the new beams. This process requires both the energy and momentum conservation to be satisfied. When the new beams also participate in other FWM processes, a series of new beams can be generated. This is the so-called cascaded FWM (CFWM). This process can widely occur in nearly all nonlinear media with broad wavelength range. Recently, CFWM has attracted more and more attention due to its wide and significant applications, including the generation of wavelength-tunable femtosecond pulses [1–3], being a multiwavelength source for dense wavelength division multiplexing systems [4], the supercontinuum generation [5,6], the optical frequency comb generation [7,8], etc.

Recently, it has been proved that the FWM process in ^{85}Rb vapor cell with a double-Λ energy-level configuration is a promising candidate for generating quantum correlation for quantum information [9–28] and quantum metrology [29–34] purposes. This system has several advantages in practical applications. First, the generated quantum correlated beams can be well separated in the spatial domain due to its nature of multispatial mode. Secondly, there is no need for cavity because of the strong nonlinearity of this FWM process. Due to these advantages in practical applications, it is worth investigating the possibility for constructing CFWM based on this system and study the quantum properties of such CFWM. In this paper, we experimentally demonstrate a CFWM process which exploits two strong pump beams crossing with each other at a small angle in the center of ^{85}Rb vapor cell. With certain crossing angle, our CFWM can emit up to 10 beams at two different frequencies. These beams show strong quantum correlation and can be well separated in the spatial domain. The number of the beams can be manipulated by altering the crossing angle of the two pump beams. We also observe such transition from 10 beams to eight beams and even to six beams. We find that the quantum correlation of our system increases as the number of the generated beams increases.

II. METHODOLOGY

A. Proposed CFWM scheme

Our proposed CFWM scheme is shown in Fig. 1(a). The two strong pump beams (Pump_1 and Pump_2) are crossed in the center of the ^{85}Rb vapor cell at a small angle. A coherent signal (seed) beam, which is redshifted from the D_1 line of the ^{85}Rb ($5S_{1/2}$, $F = 2 \rightarrow 5P_{1/2}$) [15,18,22,30] as shown in Fig. 1(b), is also injected into the ^{85}Rb vapor cell, where it symmetrically crosses with the two strong pump beams. The two strong pump beams and the signal beam are not within the same plane, making the output beams of the system well separated in the spatial domain. In this configuration, the signal beam can interact with each pump beam respectively through the normal single-pump FWM process. During two single-pump FWM processes, the signal beam ($\hat{a}_3$) is amplified and two idler beams ($\hat{a}_7$ and $\hat{a}_9$), which are blueshifted from the D_1 line of the ^{85}Rb ($5S_{1/2}$, $F = 2 \rightarrow 5P_{1/2}$) as shown in Fig. 1(b), are generated. And with the satisfaction of the energy and momentum conservation, the signal beam ($\hat{a}_3$) can also interact with both of the two pump beams simultaneously (in this sense, we could call such FWM process a dual-pump FWM interaction, in contrast with the normal single-pump FWM process), in which each pump beam annihilates one photon, the signal beam gets one photon, and the newly generated idler

*Corresponding author: jtjing@phy.ecnu.edu.cn

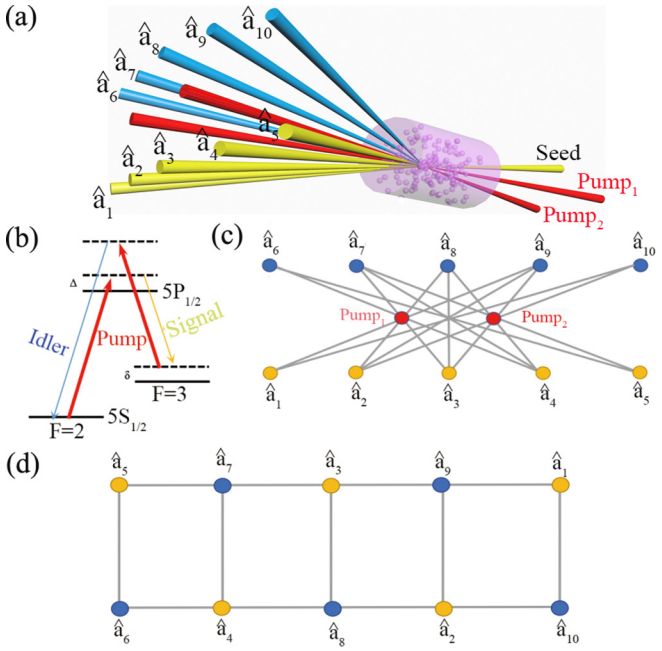

FIG. 1. Proposed two-beam pumped CFWM scheme for generating multiple-beam quantum correlation. (a) The schematic of the CFWM process. $\hat{a}_3$ is the amplified signal beam; $\hat{a}_1$, $\hat{a}_2$, $\hat{a}_4$, and $\hat{a}_5$ are the four newly generated signal beams; $\hat{a}_6$, $\hat{a}_7$, $\hat{a}_8$, $\hat{a}_9$, and $\hat{a}_{10}$ are five newly generated idler beams. (b) Energy-level diagram of ^{85}Rb D_1 line for our CFWM. Δ, one-photon detuning; δ, two-photon detuning. (c) The spatial structure of the output fields for the CFWM. (d) The simplified "ladder-type" interaction structure of the output fields for the CFWM.

beam ($\hat{a}_8$) gets the other photon. After the generation of the first three idler beams ($\hat{a}_7$, $\hat{a}_8$, and $\hat{a}_9$), the new signal beam $\hat{a}_2$ ($\hat{a}_4$) is generated by the single-pump FWM interaction between $\hat{a}_8$ and Pump$_1$ (Pump$_2$) and the dual-pump FWM interaction between $\hat{a}_9$ ($\hat{a}_7$) and both of the two pump beams. Meanwhile, the signal beam $\hat{a}_1$ ($\hat{a}_5$) is generated by the single-pump FWM interaction between $\hat{a}_9$ ($\hat{a}_7$) and Pump$_1$ (Pump$_2$). By the same token, the new idler beam $\hat{a}_6$ ($\hat{a}_{10}$) is generated by the single-pump FWM interaction between $\hat{a}_4$ ($\hat{a}_2$) and Pump$_1$ (Pump$_2$) and the dual-pump FWM interaction between $\hat{a}_5$ ($\hat{a}_1$) and both of the two pump beams. As a result, through all these single-pump and dual-pump interactions, the seed beam is amplified while four new signal beams and five new idler beams are generated. The spatial structure of the output fields from our CFWM scheme is shown in Fig. 1(c), which contains all the 13 possible FWM interactions. The two red dots mean the two pump beams (Pump$_1$ and Pump$_2$) at the output of the ^{85}Rb vapor cell. Similarly, the yellow (blue) dots mean the spatial location of the signal (idler) beams at the output of the ^{85}Rb vapor cell. The gray lines mean the interaction between the two connected beams. In this way, the connection with red dot means the single-pump FWM interaction while the connection without red dot means the dual-pump FWM interaction. And the simplified interaction structure is shown in Fig. 1(d), which omits the two pump beams (under the undepleted pump condition) and rearranges the output beams. It appears as a "ladder-type" graph, which shows the interaction structures between the beams more explicitly. Since each single-pump or dual-pump FWM interaction involved in our CFWM scheme is based on the double-Λ configuration of the ^{85}Rb D_1 line which has been demonstrated to be able to generate strongly quantum correlated beams [9–34], it is reasonable to predict that the output fields from our CFWM scheme should show quantum correlation.

B. Experimental setup

The detailed experimental layout for our two-beam pumped CFWM scheme is shown in Fig. 2(a). The system is based on the double-Λ configuration in a ^{85}Rb vapor cell. We use a cavity stabilized Ti:sapphire laser as our laser system. The frequency of the Ti:sapphire laser is blue detuned by 0.8 GHz from the ^{85}Rb D_1 line ($5S_{1/2}$, $F = 2 \rightarrow 5P_{1/2}$), which is called one-photon detuning (Δ). A polarization beam splitter (PBS) is used to divide the beam into two. The strong one is equally divided into two by a 50:50 beam splitter (BS) to

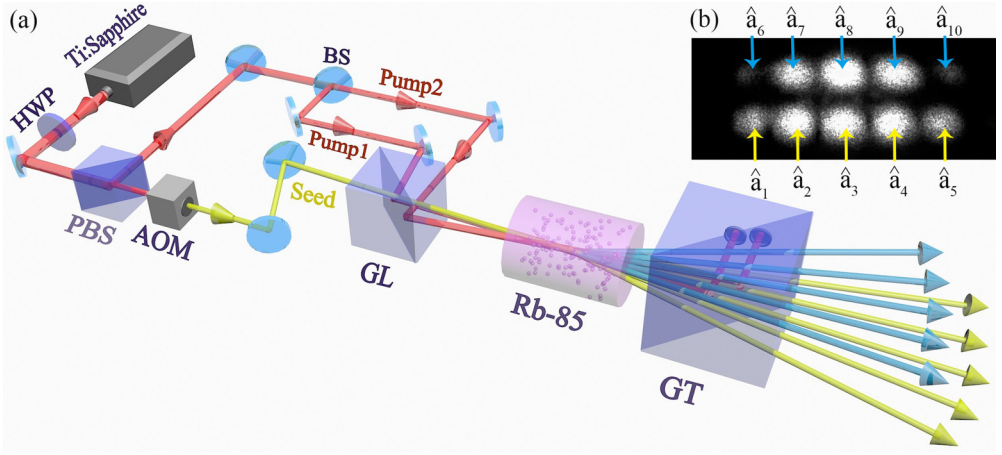

FIG. 2. Detailed experimental layout and the output fields for our CFWM scheme. (a) Detailed experimental layout for producing multiple-beam quantum correlation. HWP, half wave plate; PBS, polarization beam splitter; AOM, acousto-optic modulator; BS, beam splitter; GL, Glan-Laser polarizer; GT, Glan-Thompson polarizer; yellow lines, signal beams; blue lines, idler beams. (b) The output beams of CFWM process in the far field captured by CCD camera.

serve as the two pump beams (both Pump_1 and Pump_2 are about 100 mW). The other weak beam is passed through an acousto-optic modulator (AOM) to get the seed beam with the power of 100 μW which is red detuned by 4 MHz from the ^{85}Rb ground-state hyperfine splitting of 3.036 GHz and this is called two-photon detuning (δ). The ^{85}Rb vapor cell is 12 mm long and the temperature of the ^{85}Rb vapor cell is stabilized at 118 °C. At the center of the vapor cell, the waist of two pump beams are about 650 μm and the waist of the seed beam is about 320 μm. Combined by a Glan-Laser polarizer (GL), the two pump beams and the seed beam are crossed in the center of the ^{85}Rb vapor cell. The angle between the two pump beams is about 5.3 mrad and the seed beam is symmetrically crossed with the two pump beams. The angle between the seed beam and plane of the two pump beams is about 3.3 mrad. The two residual pump beams after the CFWM process are eliminated by a Glan-Thompson polarizer (GT) with an extinction ratio of 10^5:1 after the ^{85}Rb vapor cell. Based on these experimental settings, the generated ten beams $\hat{a}_1$, $\hat{a}_2$, $\hat{a}_3$, $\hat{a}_4$, $\hat{a}_5$, $\hat{a}_6$, $\hat{a}_7$, $\hat{a}_8$, $\hat{a}_9$, and $\hat{a}_{10}$ have powers of about 41.3 μW, 105.8 μW, 101 μW, 114 μW, 28.2 μW, 5.3 μW, 79.2 μW, 239.1 μW, 79 μW, and 4.3 μW, respectively. They are captured by the CCD camera in the far field from the ^{85}Rb vapor cell as shown in Fig. 2(b).

III. RESULTS AND DISCUSSION

A. Quantum correlation measurement

One way of observing the quantum correlation of bright beams is to measure their intensity-difference noise power spectrum and compare it with its corresponding shot-noise limit (SNL). If the intensity-difference noise power is below the SNL, we could claim that there exists quantum correlation or intensity-difference squeezing in the system [9,15,18]. Since our CFWM is based on a double-Λ configuration of ^{85}Rb vapor which has previously shown strong intensity-difference quantum correlation between the signal and idler beams [9–34], it is straightforward to divide the 10 output beams of our CFWM scheme into two groups (signal group and idler group) in order to study its quantum properties. Therefore, we send the signal group ($\hat{a}_1$, $\hat{a}_2$, $\hat{a}_3$, $\hat{a}_4$, and $\hat{a}_5$) to one photodetector and the idler group ($\hat{a}_6$, $\hat{a}_7$, $\hat{a}_8$, $\hat{a}_9$, and $\hat{a}_{10}$) to the other photodetector. The photodetectors' transimpedance gain is 10^4 V/A and the quantum efficiency is 96%. The obtained photocurrents i_1, i_2, i_3, i_4, i_5, i_6, i_7, i_8, i_9, and i_{10} indicate the photon number of beams $\hat{a}_1$, $\hat{a}_2$, $\hat{a}_3$, $\hat{a}_4$, $\hat{a}_5$, $\hat{a}_6$, $\hat{a}_7$, $\hat{a}_8$, $\hat{a}_9$, and $\hat{a}_{10}$, respectively. They are subtracted in the form of $i_1 + i_2 + i_3 + i_4 + i_5 - i_6 - i_7 - i_8 - i_9 - i_{10}$ by using a radio frequency subtractor and then analyzed by a spectrum analyzer with a setting of 30 kHz resolution bandwidth (RBW) and 300 Hz video bandwidth (VBW). This gives the noise power spectrum of the 10 beams in the form of $i_1 + i_2 + i_3 + i_4 + i_5 - i_6 - i_7 - i_8 - i_9 - i_{10}$. The result is shown in Fig. 3. The trace A (blue trace) is the normalized intensity-difference noise power spectrum in the range of 0 to 10 MHz, while the trace B (green trace) is the corresponding SNL. The black straight line at 0 dB which corresponds to the average value of data points on trace B is taken as a reference. We calibrate the SNL of the measured beams through using a coherent state beam with a power equal to the total power of the output beams impinging on the photodetectors. Then, we divide it into two beams with a 50:50 BS and send the obtained beams into the two previously used photodetectors to get the noise power of the differential photocurrent which gives the level of the corresponding SNL. As we can see, the intensity-difference noise power of the 10 beams (trace A) is about 6.7 ± 0.3 dB below the SNL (trace B) at the sideband of 2 MHz, showing a strong quantum correlation of the 10 output beams from our two-beam pumped CFWM. In other words, we have developed a two-beam pumped CFWM scheme with strong quantum correlation shared between the 10 well separated output fields. The large peaks at around 0.3 MHz and 0.7 MHz are classical noises from our Ti:sapphire laser.

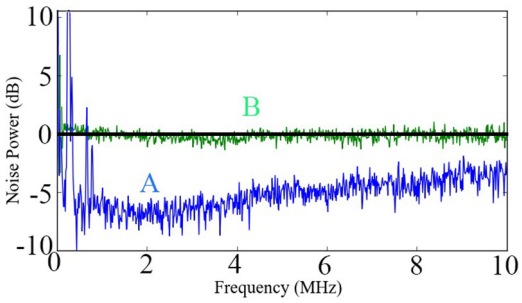

FIG. 3. Observation of multiple-beam quantum correlation from our two-beam pumped CFWM. Trace A is the intensity-difference noise power spectrum of the 10 output beams from the CFWM in the form of $i_1 + i_2 + i_3 + i_4 + i_5 - i_6 - i_7 - i_8 - i_9 - i_{10}$. Trace B is the normalized SNL. The black straight line at 0 dB is the average value of data points on trace B. The background noise and electronic noise are all about 14 dB below the SNL and have been subtracted from these two traces.

In order to study the squeezing of each signal-idler pair, we have experimentally measured the intensity-difference noise power of each signal-idler pair as shown in Fig. 4. We find that there is no intensity-difference squeezing in each signal-idler pair for our scheme. The intensity-difference noise power between $\hat{a}_3$ and $\hat{a}_8$ is closest to the SNL, which is 6 dB above the SNL. Therefore, in our system, the quantum correlation is

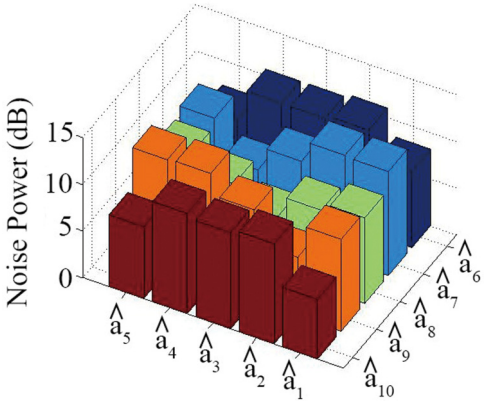

FIG. 4. Observation of the intensity-difference noise power of each signal-idler pair. The normalized SNL is 0 dB of the noise power.

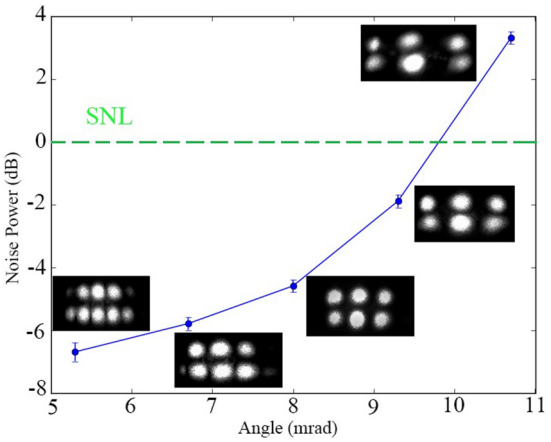

FIG. 5. Multiple-beam quantum correlation and the output fields of our CFWM versus the angle between the two pump beams. The blue dots mean the degree of squeezing or antisqueezing for our two-beam pumped CFWM scheme. The photographs of the output beams for our CFWM scheme in the far field captured by CCD camera are shown near the corresponding blue dots. The green dashed line at 0 dB is the normalized SNL.

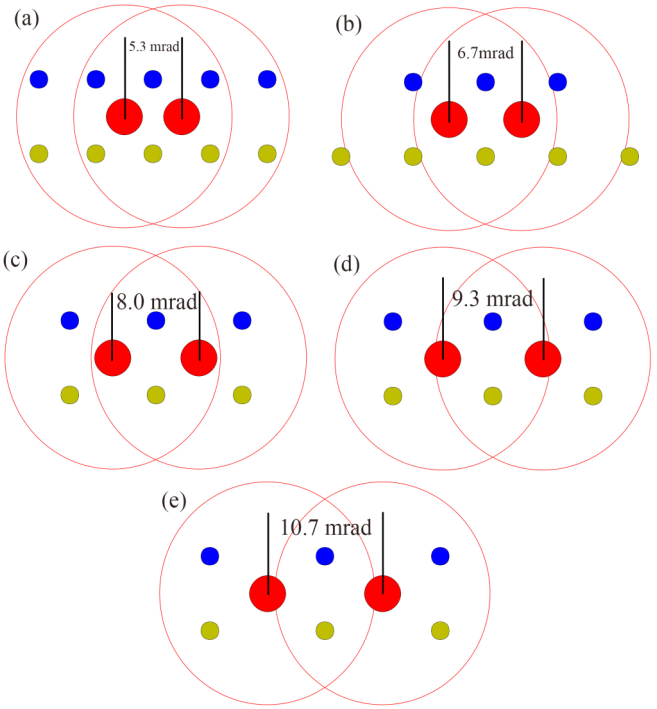

FIG. 6. Simulations of the output fields of our CFWM versus the angle between the two pump beams. They are corresponding to the five cases of the experimental results, respectively.

nonexistent in each signal-idler pair, but exists in the whole system.

B. Quantum correlation transition

Note that the above interesting results of the CFWM itself and its multiple-beam quantum correlation are only due to the introduction of an additional pump beam compared with the normal single-pump FWM process. Therefore, it is worthwhile to study how the angle between the two pump beams affects the CFWM itself and its multiple-beam quantum correlation. For this purpose, we vary the angle between the two pump beams from 5.3 mrad, 6.7 mrad, 8.0 mrad, 9.3 mrad to 10.7 mrad while keeping all the other experimental parameters the same as the aforementioned CFWM experiment. For each angle, we measure the intensity-difference noise power spectrum and its corresponding SNL, which gives us the degree of squeezing or antisqueezing shown as the blue dots in Fig. 5. The green dashed line at 0 dB is the normalized SNL. At the same time, the output beams in the far field from the ^{85}Rb vapor cell are captured by the CCD camera for each angle point as shown in Fig. 5. As we can see, we have observed the notable transition of the number of the output beams from 10 to eight, and even to six with the increase of the angle between the two pump beams. We have also found that the degree of the intensity-difference squeezing in our CFWM scheme increases as the decreasing of the angle between the two pump beams. For example, we could have quantum correlation of -6.7 ± 0.3 dB of 10 beams when the angle is 5.3 mrad. However, the quantum correlation will decrease to -5.8 ± 0.2 dB of eight beams when the angle is 6.7 mrad. Then, it will decrease to -4.6 ± 0.2 dB (-1.9 ± 0.3 dB) of six beams when the angle is 8.0 mrad (9.3 mrad). Further increasing the angle to 10.7 mrad will even make the quantum correlation of the six beams disappear (showing an antisqueezing of 3.3 ± 0.2 dB). These results can be explained as follows. The phase-matching conditions are the experimental conditions that must be satisfied for efficient FWM to occur and require the conservation of energy and momentum. In the case of the forward FWM process, the pump-signal angle is stringently set by the phase-matching conditions [35]. For the single FWM with a double-Λ energy-level configuration in our system, the phase-matching conditions are relaxed by two factors [36]. It has been proved that the pump-signal angle in the single FWM process in our system should be less than 10 mrad for the efficient FWM to occur [36]. In order to explain how the angle between the two pump beams affects the CFWM in our system, we assume that the diameter of the pump beam is roughly twice that of the signal beam. As shown in Fig. 6, the two red dots mean the two pump beams (Pump_1 and Pump_2) at the output of the ^{85}Rb vapor cell. Similarly, the yellow (blue) dot means the signal (idler) beam at the output of the ^{85}Rb vapor cell. The radius of the red circle corresponds to the maximal pump-signal angle (10 mrad). It means that only the signal and idler beams within the two red circles can be generated by our CFWM. For the pump-pump angle of 5.3 mrad shown in Fig. 6(a), there are 10 beams inside the two red circles. Therefore, the number of the output beams is 10. This corresponds to one case of the experimental results shown in Fig. 5. As we can see from the experimental result, beams $\hat{a}_6$ and $\hat{a}_{10}$ generated after the other beams are much weaker than the other beams. This may be due to their sequential order of generation. One can imagine that these two beams will disappear first if we further increase the pump-pump angle. This experimental result is actually also shown in Fig. 5. The two beams $\hat{a}_6$ and $\hat{a}_{10}$ disappear and beams $\hat{a}_1$ and $\hat{a}_5$ become much weaker than before. We also plot the simulation result of this case for the pump-pump angle of 6.7 mrad in Fig. 6(b).

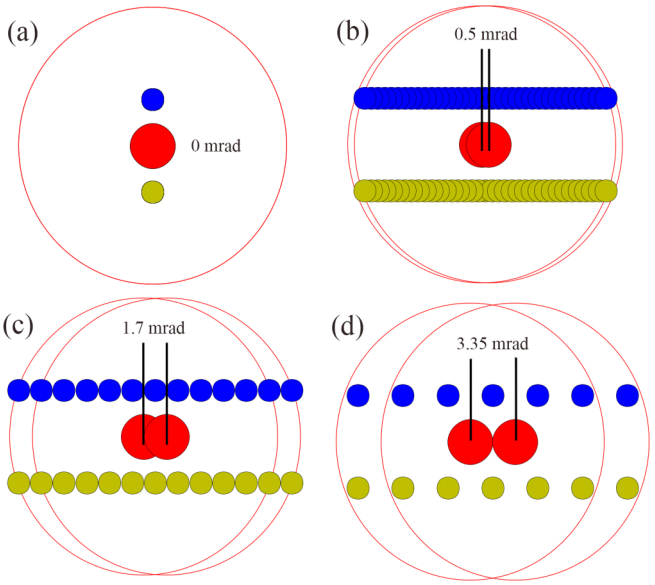

FIG. 7. Simulations of the output fields of our CFWM for the ideal case versus the angle between the two pump beams in the tiny angle region.

There are six beams inside the two red circles and two beams on the circles. Therefore, for the pump-pump angle of 6.7 mrad, the number of output beams is eight. For the pump-pump angles of 8.0 mrad [Fig. 6(c)], 9.3 mrad [Fig. 6(d)], and 10.7 mrad [Fig. 6(e)], only six beams are inside the two red circles. These results are also consistent with the experimental results shown in Fig. 5. Therefore, as the angle between the two pump beams increases, the number of output beams from our system decreases gradually. Such decrease of the interaction strength of the whole CFWM process induced by the increase of the angle between the two pump beams also explains the decrease of the multiple-beam quantum correlation as shown in Fig. 5. In addition, we consider the output fields of our CFWM for the ideal case in the tiny pump-pump angle region as shown in Fig. 7. When both pump fields are spatially degenerated as shown in Fig. 7(a), it is a normal single FWM process and the number of output beams of this system is two. Then, as shown in Fig. 7(b), when the pump-pump angle has a tiny value (0.5 mrad), the normal single FWM process is transformed into CFWM. However, the adjacent beams at the output are overlapped in this case. If we further increase the pump-pump angle to 1.7 mrad, as shown in Fig. 7(c), the output beams start to separate from each other and the number of output beams is 26. As shown in Fig. 7(d), the further increase of the angle between the two pump beams will lead to the decrease of the number of the output beams from our system. These above results of our two-beam pumped CFWM clearly show that the greater the number of the generated beams is, the stronger the quantum correlation which they share will be. It demonstrates that our system is controllable, which is beneficial to the applications.

IV. CONCLUSIONS

We have proposed a two-beam pumped CFWM scheme based on a double-Λ configuration in ^{85}Rb vapor cell and have experimentally observed the generation of up to 10 quantum correlated beams from such CFWM process. Our CFWM contains up to 13 possible single-pump or dual-pump FWM processes. During this CFWM process, the seed beam is amplified, four new signal beams and five idler beams are generated. The intensity-difference squeezing of the 10 beams from such CFWM is about -6.7 ± 0.3 dB. More interestingly, we have observed the notable transition of the number of the output beams from 10 to eight, and even to six by altering the angle between the two pump beams. With the decrease of the angle between the two pump beams, both the number of the output quantum correlated beams and their degree of quantum correlation from the two-beam pumped CFWM will increase. Our two-beam pumped CFWM system is compact, controllable, and it is easy to obtain a larger number of quantum correlated beams. The quantum correlated beams generated by our system show strong quantum correlations and can be well separated in the spatial domain. Therefore, our system may find potential applications in quantum information and quantum metrology.

ACKNOWLEDGMENTS

This paper was supported by the National Natural Science Foundation of China (Grants No. 91436211, No. 11374104, and No. 10974057), Natural Science Foundation of Shanghai (Grant No. 17ZR1442900), the Program of Scientific and Technological Innovation of Shanghai (Grant No. 17JC1400401), the Program for Professor of Special Appointment (Eastern Scholar) at Shanghai Institutions of Higher Learning, National Basic Research Program of China (Grant No. 2016YFA0302103), 111 project (Grant No. B12024), and the Fundamental Research Funds for the Central Universities.

[1] J. Liu and T. Kobayashi, Sensor **10**, 4296 (2010).
[2] W. Liu, L. Zhu, L. Wang, and C. Fang, Opt. Lett. **38**, 1772 (2013).
[3] J. Liu and T. Kobayashi, Opt. Express **16**, 22119 (2008).
[4] J. Fatome, S. Pitois, and G. Millot, IEEE J. Quantum Electron. **42**, 1038 (2006).
[5] S. T. Sørensen, C. Larsen, U. Møller, P. M. Moselund, C. L. Thomsen, and O. Bang, J. Opt. Soc. Am. B **29**, 2875 (2012).
[6] G. Genty and J. M. Dudley, IEEE J. Quantum Electron. **45**, 1331 (2009).
[7] P. Del'Haye, A. Schliesser, O. Arcizet, T. Wilken, R. Holzwarth, and T. J. Kippenberg, Nature (London) **450**, 1214 (2007).
[8] T. J. Kippenberg, R. Holzwarth, and S. A. Diddams, Science **332**, 555 (2011).
[9] C. F. McCormick, V. Boyer, E. Arimonda, and P. D. Lett, Opt. Lett. **32**, 178 (2007).
[10] C. F. McCormick, A. M. Marino, V. Boyer, and P. D. Lett, Phys. Rev. A **78**, 043816 (2008).
[11] V. Boyer, A. M. Marino, R. C. Pooser, and P. D. Lett, Science **321**, 544 (2008).

[12] A. M. Marino, V. Boyer, R. C. Pooser, P. D. Lett, K. Lemons, and K. M. Jones, Phys. Rev. Lett. **101**, 093602 (2008).
[13] A. M. Marino, R. C. Pooser, V. Boyer, and P. D. Lett, Nature (London) **457**, 859 (2009).
[14] R. C. Pooser, A. M. Marino, V. Boyer, K. M. Jones, and P. D. Lett, Phys. Rev. Lett. **103**, 010501 (2009).
[15] C. Liu, J. Jing, Z. Zhou, R. C. Pooser, F. Hudelist, L. Zhou, and W. Zhang, Opt. Lett. **36**, 2979 (2011).
[16] M. Jasperse, L. D. Turner, and R. E. Scholten, Opt. Express **19**, 3765 (2011).
[17] Q. Glorieux, L. Guidoni, S. Guibal, J.-P. Likforman, and T. Coudreau, Phys. Rev. A **84**, 053826 (2011).
[18] Z. Qin, J. Jing, J. Zhou, C. Liu, R. C. Pooser, Z. Zhou, and W. Zhang, Opt. Lett. **37**, 3141 (2012).
[19] A. MacRae, T. Brannan, R. Achal, and A. I. Lvovsky, Phys. Rev. Lett. **109**, 033601 (2012).
[20] B. J. Lawrie, P. G. Evans, and R. C. Pooser, Phys. Rev. Lett. **110**, 156802 (2013).
[21] B. J. Lawrie and R. C. Pooser, Opt. Express **21**, 7549 (2013).
[22] Z. Qin, L. Cao, H. Wang, A. M. Marino, W. Zhang, and J. Jing, Phys. Rev. Lett. **113**, 023602 (2014).
[23] U. Vogl, R. T. Glasser, J. B. Clark, Q. Glorieux, T. Li, N. V. Corzo, and P. D. Lett, New J. Phys. **16**, 013011 (2014).
[24] C. S. Embrey, M. T. Turnbull, P. G. Petrov, and V. Boyer, Phys. Rev. X **5**, 031004 (2015).
[25] M. W. Holtfrerich and A. M. Marino, Phys. Rev. A **93**, 063821 (2016).
[26] M. W. Holtfrerich, M. Dowran, R. Davidson, B. J. Lawrie, R. C. Pooser, and A. M. Marino, Optica **3**, 985 (2016).
[27] O. Danaci, C. Rios, and R. T. Glasser, New J. Phys. **18**, 073032 (2016).
[28] H. Wang, C. Fabre, and J. Jing, Phys. Rev. A **95**, 051802 (2017).
[29] A. M. Marino, N. V. Corzo Trejo, and P. D. Lett, Phys. Rev. A **86**, 023844 (2012).
[30] F. Hudelist, J. Kong, C. Liu, J. Jing, Z. Y. Ou, and W. Zhang, Nat. Commun. **5**, 3049 (2014).
[31] W. Fan, B. J. Lawrie, and R. C. Pooser, Phys. Rev. A **92**, 053812 (2015).
[32] R. C. Pooser and B. Lawrie, Optica **2**, 393 (2015).
[33] R. C. Pooser and B. J. Lawrie, ACS Photon. **3**, 8 (2016).
[34] T. Li, B. E. Anderson, T. Horrom, K. M. Jones, and P. D. Lett, Opt. Express **24**, 19871 (2016).
[35] P. Kumar and M. I. Kolobov, Opt. Commun. **104**, 374 (1994).
[36] V. Boyer, A. M. Marino, and P. D. Lett, Phys. Rev. Lett. **100**, 143601 (2008).